PERGAMON

International Journal of Solids and Structures 36 (1999) 3215–3237

INTERNATIONAL JOURNAL OF SOLIDS and STRUCTURES

Endochronic analysis for rate-dependent elasto-plastic deformation

Wen-Fung Pan*, Wu-Jiunn Chiang, Chieh-Kuen Wang

Department of Engineering Science, National Cheng Kung University, Tainan, Taiwan, 701, R.O.C.

Received 21 August 1997; in revised form 14 April 1998

Abstract

This work presents a novel formulation of the scaling function of the intrinsic time scale. The new formulated scaling function and the rate-sensitivity function are used in the endochronic theory to simulate the rate-dependent elasto-plastic behaviors of materials. Several cases of rate-dependent elasto-plastic material responses are discussed separately. Experimental data found in literature of 304 stainless steels and $Ti_7Al_2Cb_1Ta$ titanium alloy for rate-dependent elasto-plastic responses are used for comparison. It is shown that the theory adequately simulates the experimental results.

Keywords: Endochronic theory; Rate-dependent deformation; Viscoplasticity; Creep; Relaxation

1. Introduction

Experimental investigations have demonstrated that some engineering metals exhibit the rate-dependent behavior at room or elevated temperature, e.g., 304 stainless steel, 316 stainless steel, and high-strength titanium (Krempl, 1979; Kujawski and Krempl, 1981; Ikegami and Ni-Itsu, 1983; Inoue et al., 1985; Ellyin and Xia, 1991). Therefore, the study of material behavior for rate-dependent deformation is of importance in structural mechanics for engineering applications. The rate-dependent response of material should include the material response in the presence of viscoplasticity, creep, relaxation and their interactions. Although individual rate-dependent material response (viscoplasticity, creep or relaxation) has been investigated by several researchers, extremely few theoretical approaches can be used for simulating diverse rate-dependent behaviors of materials, particularly the interactions among the responses of viscoplasticity, creep and relaxation.

In the past, material behaviors of viscoplasticity, creep and relaxation were experimentally

* Corresponding author. Fax: 00 886 6 276 6549

0020–7683/99/$ - see front matter
PII: S0020–7683(98)00145–0

investigated separately (Nicholas, 1971; Yamada and Li, 1973; Krempl, 1979; Kujawski et al. 1980; Ohashi et al., 1982). Therefore, theoretical approaches were developed separately for each rate-dependent behavior. Recently, more powerful and accurate testing facilities have been used for experimentally investigating the material responses of the interactions among viscoplasticity, creep and relaxation. Kujawski and Krempl (1981) used a servocontrolled testing machine to perform experiments on a high strength, low ductility titanium alloy under repeated changes in strain rates, and short-term relaxation and creep tests. Wu and Yao (1981) experimentally observed that the creep-time curves are different at the same holding stress but for different controlled strain rate prior to creep. Yoshida (1989) tested 304 stainless steel for a certain controlled stress rate under loading and unloading condition. In his test, the step-up creep in compression was performed during the unloading process. Xia and Ellyin (1993) experimentally investigated the effects of prior plastic straining on the subsequent creep behavior of 304 stainless steel. Constant strain rates for plastic straining followed by creep tests were conducted. Wu and Ho (1993) conducted combined axial-torsional experiments to investigate the strain hardening of annealed 304 stainless steel due to creep. The strain rate dynamic loading was carefully controlled and the loading surface caused by the transient creep was studied. Wu and Ho (1995) further investigated the transient creep with a carefully monitored precreep loading stage, either loaded at a prescribed constant strain rate or at a constant stress rate. Due to part of the rate-dependent responses for the aforementioned experimental data, theoretical approaches were also restricted to simulate a portion of the rate-dependent responses of material. However, a complete theoretical model for rate-dependent deformation should cover the simulation for all kinds of rate-dependent behaviors of materials.

By using the plastic strain tensor to define the intrinsic time measure (Valanis, 1980), the endochronic theory has been extensively used to describe various materials subjected to diverse loading histories (Wu and Yip, 1981; Valanis and Lee, 1984; Watanabe and Atluri, 1985; Valanis and Read, 1986; Murakami and Read, 1987; Wu et al., 1990; Imai and Xie, 1990; Fan and Peng, 1991; Mathison et al., 1991; Peng and Ponter, 1993; Lee, 1994; Wu et al., 1995; Pan et al., 1996). Endochronic theory has also been extended to investigate part of the rate-dependent behaviors of materials. Lin and Wu (1976) introduced a rate-sensitivity function, which is a function of total strain rate. The function was applied to examine the material behavior for uniaxial strain rate effect. Wu and Yip (1980) redefined the rate-sensitivity function of the intrinsic time measure based on the new definition of the intrinsic time measure proposed by Valanis (1980). The uniaxial stress–strain responses of 1100-O aluminum and mild steel at various constant stain rate conditions were theoretically discussed. Lin and Wu (1983) upgraded the rate-sensitivity function and investigated the material response under different strain rate cases. Moreover, the derived constitutive equations were applied to the viscoplastic wave-propagation problem of a thin-walled tube subjected to impact loading. Watanabe and Atluri (1986) introduced a formulation of the scaling function of the intrinsic time scale, as was initially suggested by Valanis (1975). The material behavior of creep for type-304 stainless steel at elevated temperature were discussed in their study. Wu and Ho (1995) proposed a different formulation of the scaling function of the intrinsic time scale. The endochronic theory was applied to investigate the transient creep with a carefully monitored precreep loading stage, either loaded at a prescribed constant strain rate or at a constant stress rate. Lee (1996) used a new formulation of the intrinsic time measure to investigate the transient creep of metals for variable temperature. The creep under step-up and step-down temperatures with a constant axial stress for SUS 304 stainless steel were studied in their research. Pan and

Chern (1997) proposed a new formulation of the rate-sensitivity function by using the equivalent plastic strain rate. The theory was extended to describe the viscoplastic behavior of material subjected to multiaxial loading. By considering the total strain rate during the simulation process, the stress–strain response for a small strain range or in transition area of the changing loading direction can be properly described. Pan and Leu (1997) extended the formulation of the rate-sensitivity function proposed by Pan and Chern (1997) to examine the viscoplastic collapse of thin-walled tubes subjected to pure bending. The relationship among moment, curvature and ovalization of thin-walled tubes for different curvature rates was discussed in their study. Furthermore, Pan (1997) modified the rate-sensitivity function, which was proposed by Pan and Chern (1997), to incorporate with the finite endochronic constitutive equation obtained by Pan et al. (1996) to investigate the material responses subjected to finite viscoplastic deformation. The simulated shear stress–strain responses and the axial effects caused by the finite torsion correlate well with the experimental data.

In this paper, a different formulation of the scaling function of the intrinsic time measure, as was initially suggested by Valanis (1975), is proposed to describe the material behaviors under rate-dependent elasto-plastic deformation. The rate-sensitivity function derived from Pan and Chern (1997) and the differential endochronic constitutive equations (derived by Valanis, 1984); Murakami and Read, 1989; Pan et al., 1996; Pan and Chern, 1997) are used in this study. A unified endochronic theory is constructed with can be used for describing the material behaviors under all kinds of the rate-dependent elasto-plastic deformation. The difference between our work and the theoretical work of Wu and Ho (1995) are: (i) The proposed scaling function can be used in the endochronic constitutive equations without yield condition to simulate the rate-dependent elasto-plastic behavior of materials, and (ii) the rate-sensitivity function used in this paper is the formulation proposed by Pan and Chern (1997). To evaluate the proposed theoretical approach, experimental data for rate-dependent behavior of 304 stainless steels and $Ti_7Al_2Cb_1Ta$ titanium alloy found in previous literature are used to compare with the theoretical simulation. Experimental data for this investigation include the following: material responses of (i) viscoplasticity and viscoplasticity–relaxation interaction for $Ti_7Al_2Cb_1Ta$ titanium alloy tested by Kujawski and Krempl (1981), (ii) viscoplasticity and viscoplasticity–creep interaction for SUS 304 stainless steel tested by Yoshida (1989), and (iii) viscoplasticity and viscoplasticity–creep interaction for annealed 304 stainless steel tested by Wu and Ho (1995). Comparison with the experimental results reveals that most of the rate-dependent elasto-plastic behaviors of materials can be adequately simulated by our endochronic approach.

2. The endochronic theory

Under conditions of small deformation, isotropic and plastically incompressible, the endochronic constitutive equations are expressed as follows (Valanis, 1980):

$$\underset{\sim}{S} = 2\int_0^z \rho(z-z')\frac{\partial \underset{\sim}{e}^p}{\partial z'}\,\mathrm{d}z' \tag{1}$$

in which

$$\mathrm{d}\underset{\sim}{e}^{p} = \mathrm{d}\underset{\sim}{e} - \frac{\mathrm{d}\underset{\sim}{s}}{2\mu_0} \tag{2}$$

and z is the intrinsic time scale, $\underset{\sim}{s}$ is the deviatoric stress, $\underset{\sim}{e}$ is the deviatoric strain, and μ_0 is the elastic shear modulus. The kernel function $\rho(z)$ in the above linear functional representation of stress possesses a weak singularity at the origin and is integrable in region of $0 < z < \infty$ (Valanis, 1980), i.e.,

$$\rho(0) = \infty \tag{3}$$

and

$$\int_0^z \rho(z')\mathrm{d}z' < \infty \tag{4}$$

The kernel function $\rho(z)$ is approximated with a finite sum of exponentially decaying function, as indicated from previous mathematical character, which is

$$\rho(z) \cong \sum_{r=1}^{n} C_r \mathrm{e}^{-\alpha_r z}; \quad \rho(0) = \sum_{r=1}^{n} C_r = \text{large number} \tag{5a,b}$$

where C_r and α_r are material constants. Substitution of eqn (5a) into eqn (1) leads to:

$$\underset{\sim}{s} = \sum_{r=1}^{n} \underset{\sim}{s}_r \tag{6}$$

where

$$\underset{\sim}{s}_r = 2C_r \int_0^z e^{-\alpha_r(z-z')} \frac{\partial \underset{\sim}{e}^{\mathrm{p}}}{\partial z'} \mathrm{d}z'. \tag{7}$$

According to the Leibniz's differential rule, eqn (7) becomes the following linear first-order differential equations (Valanis, 1984; Murakami and Read, 1989; Pan et al., 1996; Pan and Chern, 1997):

$$\frac{\mathrm{d}\underset{\sim}{s}_r}{\mathrm{d}z} + \alpha_r \underset{\sim}{s}_r = 2C_r \frac{\mathrm{d}\underset{\sim}{e}^{\mathrm{p}}}{\mathrm{d}z}, \quad r = 1, 2, \ldots, n \tag{8}$$

and

$$\mathrm{d}\underset{\sim}{s} = \sum_{r=1}^{n} \mathrm{d}\underset{\sim}{s}_r = 2\sum_{r=1}^{n} C_r \mathrm{d}\underset{\sim}{e}^{\mathrm{p}} - \sum_{r=1}^{n} \alpha_r \underset{\sim}{s}_r \mathrm{d}z. \tag{9}$$

The intrinsic time measure ζ is defined as

$$\mathrm{d}\zeta = k\| \mathrm{d}\underset{\sim}{e}^{\mathrm{p}} \| \quad \text{or} \quad \mathrm{d}\zeta^2 = k^2 \mathrm{d}\underset{\sim}{e}^{\mathrm{p}} \cdot \mathrm{d}\underset{\sim}{e}^{\mathrm{p}} \tag{10a,b}$$

in which $\| \cdot \|$ represents the Euclidean norm, and k is the rate-sensitivity function which can be used for describing the viscoplastic behavior of material. The intrinsic time scale z is (Valanis, 1975)

$$dz^2 = \left(\frac{d\zeta}{f(\zeta)}\right)^2 + g^2 dt^2 \tag{11}$$

where g denotes a scaling function which can be used for describing the material behavior under creep or relaxation, t is the Newtonian time, and $f(\zeta)$ is a material hardening function which can be expressed as

$$f(\zeta) = 1 - Ce^{-\beta\zeta}, \quad \text{for } C < 1 \tag{12}$$

in which C and β are material parameters. If the plastic incompressibility is satisfied, the elastic hydrostatic response can be expressed as

$$d\sigma_{kk} = 3K d\varepsilon_{kk} \tag{13}$$

where σ_{kk} and ε_{kk} denote the trace of stress and strain tensors, and K is the elastic bulk modulus. Note that the rate-sensitivity function k is treated as unity and the scaling function g is treated as zero to describe rate independent material behavior. Furthermore, the plastic strain tensor from eqns (1)–(10) is changed to creep strain tensor and inelastic strain tensor if the theory is extended to investigate the material behavior under creep and relaxation, respectively. Figure 1(a) and (b) schematically depict the variation of the creep strain $\varepsilon_1^{\,c}$ for uniaxial creep and inelastic strain $\varepsilon_1^{\,IN}$ for uniaxial relaxation, respectively. The endochronic theory for rate-dependent elasto-plastic deformation is discussed separately as follows.

2.1. Viscoplasticity

To describe the material viscoplastic behavior, Wu and Yip (1980) introduced a formulation of the rate-sensitivity function k to simulate the material behavior for uniaxial strain-rate and its history effect. It is expressed as

$$k = 1 - k_a \log\left[\frac{\dot{e}_1^p}{(\dot{e}_1^p)_o}\right] \tag{14}$$

where $(\dot{e}_1^p)_o$ denotes the reference uniaxial deviatoric plastic strain rate, $\dot{e}_1^p$ represents the relative uniaxial deviatoric plastic strain rate, and k_a is a rate-sensitivity parameter. The uniaxial stress–strain responses of 1100-O aluminum and mild steel at various constant strain rate conditions were theoretically discussed in their study. Lin and Wu (1983) modified the formulation of rate-sensitivity function to be

$$k = 1 - k_a \log\left[\frac{\dot{e}_1^p}{(\dot{e}_1^p)_o}\right] - k_b \log\left[\frac{\dot{e}_1^p}{(\dot{e}_1^p)_o}\right]^2 \tag{15}$$

where k_b denotes the second-order rate-sensitivity parameter. This form of the rate-sensitivity function was applied to investigate the viscoplastic wave-propagation problem of a thin-walled tube subjected to impact loading. Pan and Chern (1997) proposed a formulation of function k to describe the viscoplastic behavior of material subjected to multiaxial loading. The function k is expressed as

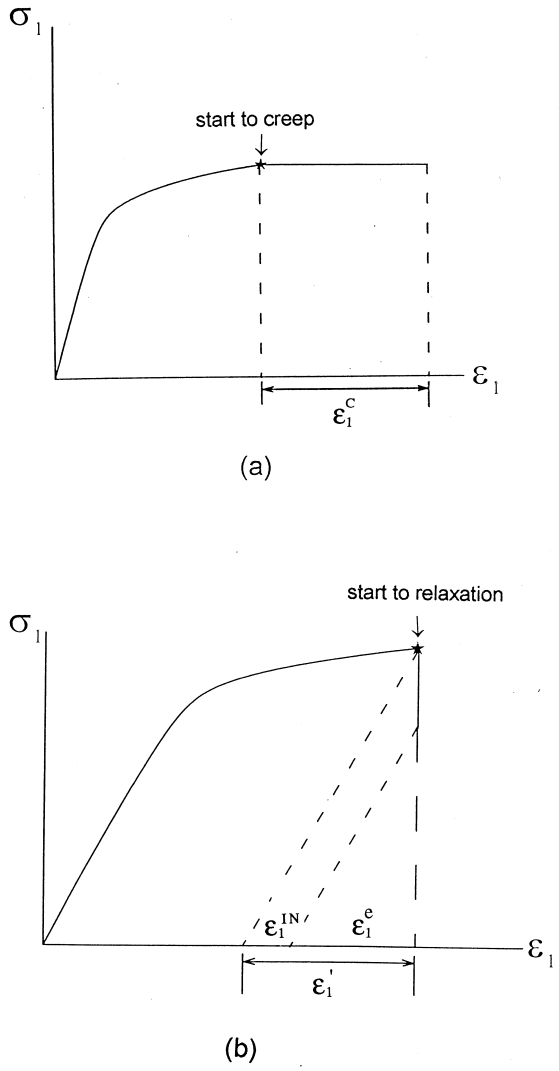

Fig. 1. Schematic drawings of the uniaxial stress–strain curve for (a) creep and (b) relaxation.

$$k = 1 - k_a \log\left[\frac{\dot{e}^p_{eq}}{(\dot{e}^p_{eq})_o}\right] \tag{16}$$

where k_a denotes a rate-sensitivity parameter, $(\dot{e}^p_{eq})_o$ is the reference equivalent deviatoric plastic strain rate, and $\dot{e}^p_{eq}$ is the relative equivalent deviatoric plastic strain rate. By considering the total strain rate during the simulation process, the stress–strain response for a small strain range or in transition area of the changing loading direction can be properly described. Theoretical simulations of uniaxial loading, combined axial-torsional loading and biaxial loading with various strain rate or stress rate cases for 304 stainless steel correlated well with the experimental data in their study.

2.2. Creep or viscoplasticity-creep interaction

To describe the material behavior under creep, the increment of the deviatoric creep strain tensor $\underset{\sim}{e}^{c}$ from eqn (2) is expressed as

$$\mathrm{d}\underset{\sim}{e}^{c} = \mathrm{d}\underset{\sim}{e} - \frac{\mathrm{d}\underset{\sim}{s}}{2\mu_0}. \tag{17}$$

The increment of deviatoric stress tensor from eqn (9) is

$$\mathrm{d}\underset{\sim}{s} = \sum_{r=1}^{n} \mathrm{d}\,\underset{\sim}{s}_r = 2\sum_{r=1}^{n} C_r\,\mathrm{d}\,\underset{\sim}{e}^{c} - \sum_{r=1}^{n} \alpha_r s_r\,\mathrm{d}z. \tag{18}$$

The intrinsic time measure ζ for creep is defined at

$$\mathrm{d}\zeta = k\|\,\mathrm{d}\underset{\sim}{e}^{c}\| \quad \text{or} \quad \mathrm{d}\zeta^2 = k^2\,\mathrm{d}\underset{\sim}{e}^{c}\cdot\mathrm{d}\underset{\sim}{e}^{c}. \tag{19a,b}$$

Watanabe and Atluri (1986) formulated the scaling function g to investigate the material behavior under creep, which is

$$g = \frac{f(\zeta)}{B}\left(\frac{\|\underset{\sim}{s}-\underset{\sim}{r}\|}{\tau_y^{o} f}\right)^{1-m} \tag{20}$$

in which $\underset{\sim}{r}$ denotes the back stress tensor, τ_y^{o} represents the initial yield stress in shear, B and m are material parameters. They investigated the creep–plasticity interaction for type-304 stainless steel at elevated temperature. To describe the material behavior under viscoplasticity–creep interaction, the rate-sensitivity function k has to be used. Wu and Ho (1995) proposed the scaling function g as

$$g = B\sqrt{1-k^2\,\frac{\|\underset{\sim}{s}-\underset{\sim}{r}\|}{(s_y^{o} f)^2}} \tag{21}$$

where s_y^{o} denotes the yield stress at a reference plastic strain rate (usually the lowest strain rate in the test), B is a scaling function which is defined as

$$B = \frac{b s_y^{o}}{\|\underset{\sim}{s}-\underset{\sim}{r}\|}\left(\frac{k\|\underset{\sim}{s}-\underset{\sim}{r}\|}{s_y^{o} f}\right)^{m} \tag{22}$$

in which b and m are material parameters. The substitution of eqn (21) into eqn (11) yields

$$\mathrm{d}z = B\,\mathrm{d}t. \tag{23}$$

When the material function $f(\zeta)$ equals 1, the magnitude of b can be shown to be the initial creep rate. The material behavior of viscoplasticity–creep interaction for 304 stainless steel were also experimentally investigated by Wu and Ho (1995).

Herein, a different formulation of the scaling function g without any yield condition is proposed as

$$g = \sqrt{b^2 \left(\frac{k \left\| \sum_{r=1}^{n} \alpha_r \underset{\sim}{s}_r \right\|}{\rho(0) f(\zeta)} \sum_{r=1}^{n} \mathrm{e}^{-\alpha_r \zeta} \right)^{2m} - \frac{\zeta^2}{f^2}} \tag{24}$$

where m denotes a material parameter, and b represents a parameter which is related to the last strain rate before creep. Substituting eqn (24) into eqn (11), an equation, which is the same as eqn (23), is obtained. However, the quantity of B is

$$B = b \left(\frac{k \left\| \sum_{r=1}^{n} \alpha_r \underset{\sim}{s}_r \right\|}{\rho(0) f(\zeta)} \sum_{r=1}^{n} \mathrm{e}^{-\alpha_r \zeta} \right)^{m}. \tag{25}$$

We now discuss the determination of the quantity b in eqn (25). If we consider a case of uniaxial viscoplasticity–creep interaction, the increments of the total and deviatoric stress tensors and creep strain tensor can be expressed as

$$\mathrm{d}\underset{\sim}{\sigma} = \mathrm{d}\underset{\sim}{s} = \begin{bmatrix} 0 & 0 & 0 \\ 0 & 0 & 0 \\ 0 & 0 & 0 \end{bmatrix}, \mathrm{d}\underset{\sim}{\varepsilon}^{\mathrm{c}} = \begin{bmatrix} \mathrm{d}\varepsilon_1^{\mathrm{c}} & 0 & 0 \\ 0 & \mathrm{d}\varepsilon_2^{\mathrm{c}} & 0 \\ 0 & 0 & \mathrm{d}\varepsilon_2^{\mathrm{c}} \end{bmatrix}. \tag{26a,b}$$

If the assumption of incompressible condition is satisfied under creep, one writes

$$\mathrm{d}\varepsilon_1^{\mathrm{c}} = -2\mathrm{d}\varepsilon_2^{\mathrm{c}}. \tag{27}$$

Thus, the increment of the deviatoric creep strain tensor $\mathrm{d}\underset{\sim}{e}^{\mathrm{c}}$ is determined to be

$$\mathrm{d}\underset{\sim}{e}^{c} = \mathrm{d}\underset{\sim}{\varepsilon}^{c}. \tag{28}$$

From eqn (28), eqn (18) is written as

$$\mathrm{d}\underset{\sim}{s} = \sum_{r=1}^{n} \mathrm{d}\,\underset{\sim}{s}_r = 2\rho(0)\mathrm{d}\underset{\sim}{\varepsilon}^{\mathrm{c}} - \sum_{r=1}^{n} \alpha_r s_r \,\mathrm{d}\,z. \tag{29}$$

Substitution of eqns (26a) and (26b) into eqn (29) yields

$$\dot{z} = \frac{2\rho(0)\dot{\varepsilon}_1^{\mathrm{c}}}{\sum_{r=1}^{n} \alpha_r (s_1)_r} \tag{30}$$

From eqns (23) and (25), the quantity of $\dot{z}$ is

$$\dot{z} = b \left(\frac{k \left\| \sum_{r=1}^{n} \alpha_r \underset{\sim}{s}_r \right\|}{\rho(0) f(\zeta)} \sum_{r=1}^{n} \mathrm{e}^{-\alpha_r \zeta} \right)^{m}. \tag{31}$$

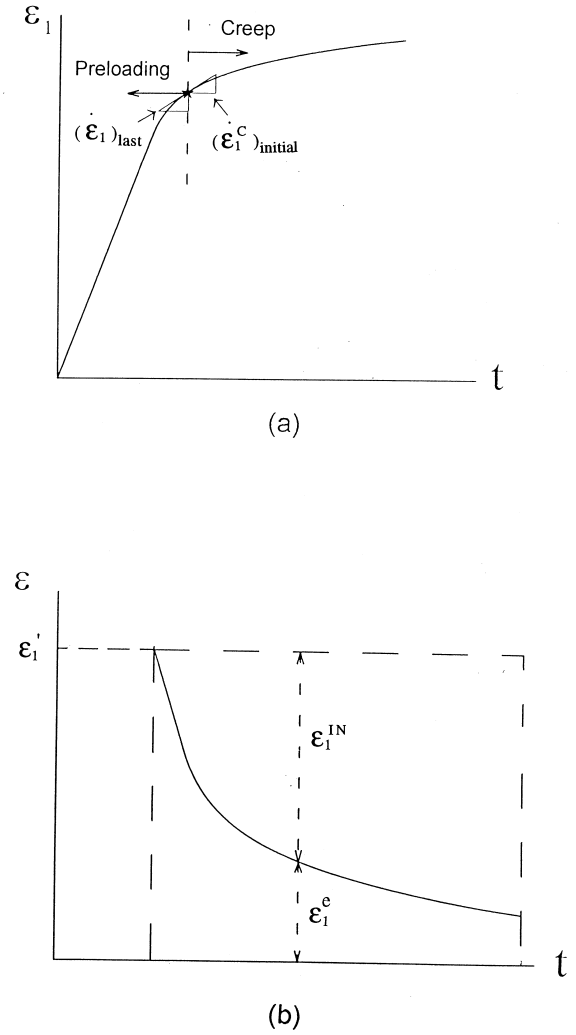

Fig. 2. Schematic drawings of the uniaxial strain–time curve for (a) creep and (b) relaxation.

From Fig. 2(a), the initial creep strain rate $(\dot{\varepsilon}_1^c)_{\text{initial}}$ is a continuation of the last preloading strain rate $(\dot{\varepsilon}_1)_{\text{last}}$ before creep for uniaxial creep test (Wu and Ho, 1995). Thus,

$$(\dot{\varepsilon}_1)_{\text{last}} = (\dot{\varepsilon}^c)_{\text{initial}}. \tag{32}$$

The quantity of $\left\| \sum_{r=1}^{n} \alpha_r \underset{\sim}{s}_r \right\|$ is a known value which is related to the last stress condition before creep, and ζ is also the known magnitude of the last intrinsic time measure before creep. Once the strain rate before creep $(\dot{\varepsilon}_1)_{\text{last}}$ is determined, the quantity of $(\dot{\varepsilon}_1^c)_{\text{initial}}$ is also known from eqn (32) and the magnitude of b can be determined from eqns (30) and (31).

2.3. Viscoplasticity–relaxation interaction

We now discuss the determination of b for the case of viscoplasticity–relaxation interaction. If we consider a case of uniaxial viscoplasticity–relaxation interaction, increments of the total and deviatoric strain tensors are expressed as

$$\mathrm{d}\underset{\sim}{\varepsilon} = \mathrm{d}\underset{\sim}{e} = \begin{bmatrix} 0 & 0 & 0 \\ 0 & 0 & 0 \\ 0 & 0 & 0 \end{bmatrix} \tag{33}$$

The incremental inelastic strain tensor $\mathrm{d}\underset{\sim}{\varepsilon}^{\mathrm{IN}}$ is expressed as

$$\mathrm{d}\underset{\sim}{\varepsilon}^{\mathrm{IN}} = \begin{bmatrix} \mathrm{d}\varepsilon_1^{\mathrm{IN}} & 0 & 0 \\ 0 & \mathrm{d}\varepsilon_2^{\mathrm{IN}} & 0 \\ 0 & 0 & \mathrm{d}\varepsilon_2^{\mathrm{IN}} \end{bmatrix}. \tag{34}$$

Figure 1(b) depicts the inelastic strain change due to the stress relaxation for uniaxial loading. The magnitude of ε_1' is a constant during relaxation and it can be decomposed into changeable elastic strain $\varepsilon_1^{\mathrm{e}}$ and inelastic strain $\varepsilon_1^{\mathrm{IN}}$. Figure 2(b) schematically shows the variation of the inelastic strain $\varepsilon_1^{\mathrm{IN}}$. If the assumption of incompressible condition is satisfied for the inelastic deformation, one obtained

$$\mathrm{d}\varepsilon_1^{\mathrm{IN}} = -2\mathrm{d}\varepsilon_2^{\mathrm{IN}}. \tag{35}$$

Thus, the deviatoric incremental inelastic strain tensor $\mathrm{d}\underset{\sim}{e}^{\mathrm{IN}}$ is

$$\mathrm{d}\underset{\sim}{e}^{\mathrm{IN}} = \mathrm{d}\underset{\sim}{\varepsilon}^{\mathrm{IN}}. \tag{36}$$

Substitution of eqns (33) and (34) into eqn (17) yields

$$\mathrm{d}\underset{\sim}{s} = -2\mu_0\, \mathrm{d}\underset{\sim}{e}^{\mathrm{IN}}. \tag{37}$$

Substituting eqn (37) into eqn (18), one obtains

$$2(\rho(0)+\mu_0)\, \mathrm{d}\underset{\sim}{e}^{\mathrm{IN}} = \sum_{r=1}^{n} \alpha_r \underset{\sim}{s}_r\, \mathrm{d}z. \tag{38}$$

By using eqns (34), (36) and (37), eqn (38) becomes

$$\dot{z} = \frac{2(\rho(0)+\mu_0)\dot{\varepsilon}_1^{\mathrm{IN}}}{\sum_{r=1}^{n} \alpha_r (s_1)_r} \tag{39}$$

Based on the variation of the inelastic strain $\varepsilon_1^{\mathrm{IN}}$ from Fig. 2(b), we assume that the initial inelastic

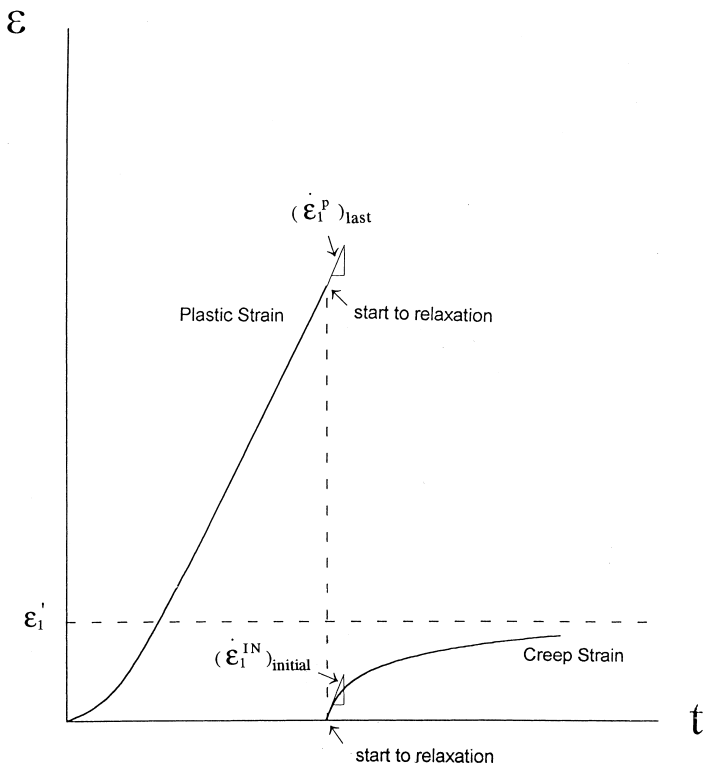

Fig. 3. Schematic drawing of uniaxial plastic strain–time and creep strain–time curves for relaxation.

strain rate $(\dot{\varepsilon}_1^{IN})_{initial}$ is a continuation of the last plastic strain rate before relaxation $(\dot{\varepsilon}_1^{p})_{last}$ (see Fig. 3). Thus,

$$(\dot{\varepsilon}_1^{p})_{last} = (\dot{\varepsilon}_1^{IN})_{initial}. \tag{40}$$

From eqns (22) and (23), the quantity of $\dot{z}$ is the same as eqn (31). The quantity of $\left\| \sum_{r=1}^{n} \alpha_r \underset{\sim}{S}_r \right\|$ is a known value which is related to the last stress condition before relaxation, ζ is also the known magnitude of the last intrinsic time measure before relaxation. Once the plastic strain rate before relaxation $(\dot{\varepsilon}_1^{p})_{last}$ is determined, the quantity of $(\dot{\varepsilon}_1^{IN})_{initial}$ is also known from eqn (40) and the magnitude of b can be determined from eqns (39) and (31).

3. Comparison and discussion of the theoretical and experimental results

In this section, theoretical results are compared with experimental data obtained by Kujawski and Krempl (1981), Yoshida (1989) and Wu and Ho (1995). Tested materials include $Ti_7Al_2Cb_1Ta$

Table 1
Material parameters for 304 stainless steels and $Ti_7Al_2Cb_1Ta$ titanium alloy

μ_0(MPa)	K(MPa)	C_1(MPa)	C_2(MPa)	C_3(MPa)	α_1	α_2	α_3	C	β	K_a	m
304 Stainless steel (Yoshida)											
64,000	160,830	6.18×10^5	1.04×10^4	2.4×10^3	6240	500	90	0.33	9.2	0.0585	5.7
304 Stainless steel (Wu and Ho)											
69,550	181,370	5.5×10^5	4.45×10^3	2.05×10^3	6120	450	80	0.33	9.2	0.0585	5.3
$Ti_7Al_2Cb_1Ta$ Titanium alloy (Kujawski and Krempl)											
41,790	195,000	1.23×10^6	9.9×10^3	6.0×10^3	3661	700	120	0.22	2.2	0.021	10.3

titanium alloy and 304 stainless steels for rate-dependent elasto-plastic responses. Material parameters for the theory derived in the previous section are determined according to the method proposed by Fan (1983). It is found that the material behaviors of 304 stainless steel tested by Yoshida (1989) and Wu and Ho (1995) are different, as indicated from the uniaxial stress–strain curves at the strain rate of 10^{-6} s^{-1}. Therefore, two different groups of material parameters are required. Table 1 lists the material parameters for $Ti_7Al_2Cb_1Ta$ titanium alloy and 304 stainless steels. Based on the experimental data, different rate-dependent elasto-plastic behaviors are discussed separately.

3.1. Viscoplasticity

Figure 4 depicts the viscoplastic behavior of SUS 304 stainless steel in reversed loading at various strain rates tested by Yoshida (1989). In their tests, the strain rate was changed or unchanged at the strain reversal point in four different ways, with are $\dot{\varepsilon} = 10^{-6}$–$10^{-2}$ s^{-1}; 10^{-6}–10^{-6} s^{-1}; 10^{-2}–10^{-2} s^{-1}; and 10^{-2}–10^{-6} s^{-1}. The corresponding simulated results are also shown in Fig. 4 in the solid line. Similar investigation on annealed commercially pure aluminum in the strain rate range from 10^{-4} to 10^{3} s^{-1} and mild steel in the strain-rate range from 10^{-4} to 10^{-1} was also discussed by Wu and Yip (1980). The viscoplastic behavior of 304 stainless steel for different constant strain rates tested by Wu and Ho (1995) is shown in Fig. 5(a). The strain rates were set at 2×10^{-6}, 10^{-5}, 10^{-4} and 10^{-3} s^{-1}. Figure 5(b) depicts the simulated result. Figure 6 shows the experimental and theoretical data of the viscoplastic behavior for 304 stainless steel under two different constant stress rates of 2.07 and 20.7 MPa s^{-1}, respectively. The experimental results are also tested by Wu and Ho (1995). Figure 7(a) shows the viscoplastic behavior of $Ti_7Al_2Cb_1Ta$ titanium alloy in the loading and unloading stress–strain curve for different strain rate or stress rates tested by Kujawski and Krempl (1981). Four stages of the controlled strain rate or stress rates for the loading process were the strain rate of 10^{-5} s^{-1} for stage 1 and stress rate of 21.7, 2.17 and 0.217 MPa s^{-1} for stages 2–4, respectively. Figure 7(b) shows the simulated result. These figures confirm that the theoretical prediction for viscoplastic behavior of materials correlates well with the experimental result.

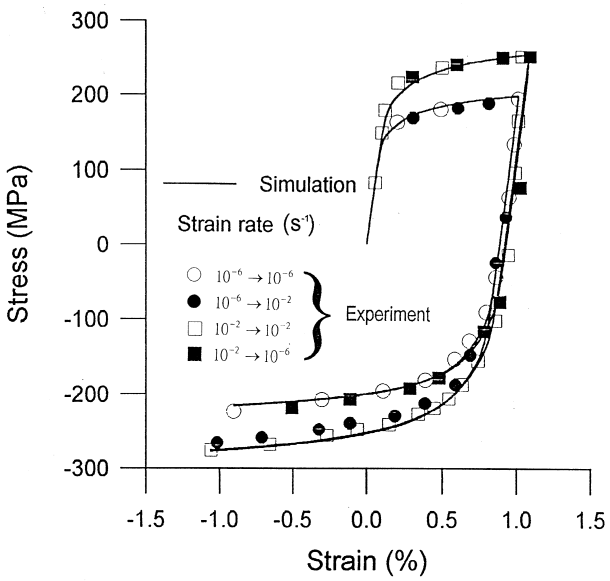

Fig. 4. Experimental and theoretical axial stress–strain curves for 304 stainless steel at changed or unchanged strain rates.

3.2. Viscoplasticity–creep interaction

Yoshida (1989) tested the viscoplasticity–creep interaction for SUS 304 stainless steel under the controlled stress rate of 30 MPa s^{-1} at room temperature. Three stages of creep were conducted when the specimen was unloaded, as shown in Fig. 8. Each stage was under creep for 10 h with the holding stresses of -150, -200 and -230 MPa, respectively. The simulated curve is also indicated in Fig. 8. Wu and Ho (1995) also tested on 304 stainless steel for material behavior of viscoplasticity–creep interaction. Figure 9 displays the creep curves of various constant strain rates preloading at the same holding stress of 206.7 MPa. It is shown that the higher creep strain is observed when the preloading strain rate is faster. The theoretical simulation is depicted by a solid line. Figure 10 demonstrate the creep curves of two constant stress rates (2.07 and 20.7 MPa s^{-1}) preloading at the same holding stress of 206.7 MPa. According to this figure, the higher creep strain implies a faster stress rate. Figure 11 demonstrates the creep strain vs time curves of the two creep stages, each having a different holding stress; however, both have the same preloading stress rate (20.7 MPa s^{-1}) during their preloading or reloading stage. It is seen that the curve of the holding stress at 234.26 MPa is higher than that of holding stress at 206.7 MPa. Figure 12(a) shows the experimental stress–strain curves with loadings of two constant stress rates (2.07 and 20.7 MPa s^{-1}). Each curve consists of two creep stages. The first creep stage had a holding stress of 206 MPa and lasted for 60 min; and the second creep stage had a holding stress 234.26 MPa and also lasted for 60 min. Figure 12(b) depicts the simulated results. Figure 13(a) and (b) show the experimental and simulated results of the unloading/reloading response following elasto-plastic deformation by a solid line and the unloading/reloading response following creep by a dotted line. It is shown that good agreement between the theoretical and experimental results has been achieved.

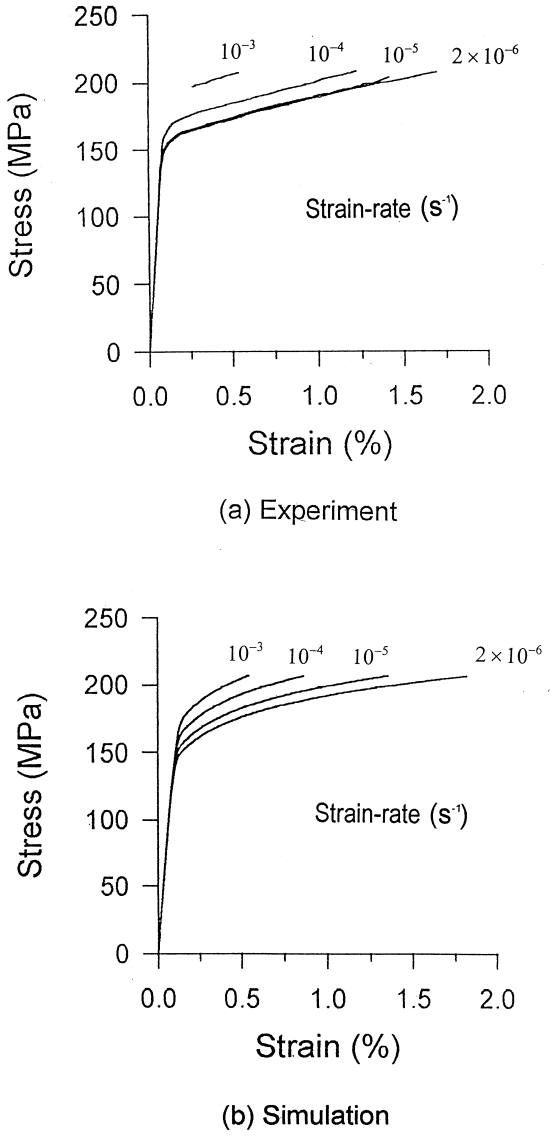

Fig. 5. Experimental and theoretical axial stress–strain curves for 304 stainless steel at different strain rates.

3.3. Viscoplasticity–relaxation interaction

The experimental data of the viscoplasticity–relaxation interaction for $Ti_7Al_2Cb_1Ta$ titanium alloy tested by Kujawski and Krempl (1981) are shown in Fig. 14. In their test, the specimen was monotonic loaded with a prestrain of 3.25%. The relaxation was induced for 10 min and subsequent reloading at various strain rates ranging for 10^{-3} to 10^{-7} s^{-1}. It is evident that the total stress drop

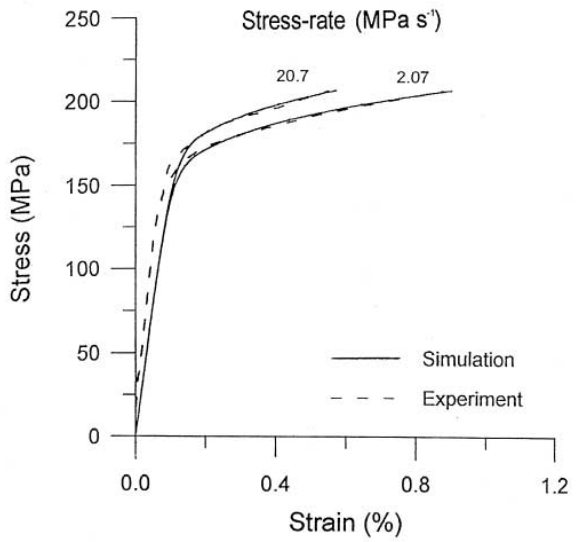

Fig. 6. Experimental and theoretical axial stress–strain curves for 304 stainless steel at different stress rates.

depends on the strain rate preceding the relaxation tests. It is independent of the stress and the strain at the start of the relaxation tests. A comparison with the experimental data is also revealed in Fig. 14. This figure confirms that the theoretical approach satisfactorily describes the experimental result.

4. Conclusion

This paper presents a formulation of the scaling function of the intrinsic time scale. The proposed scaling function and the rate-sensitivity function introduced by Pan and Chern (1997) can be used with the endochronic differential constitutive equations (derived by Valanis, 1984; Murakami and Read, 1989; Pan et al., 1996; Pan and Chern, 1997) to describe the material responses subjected to rate-dependent elasto-plastic deformation. In our study, several cases of rate-dependent elasto-plastic material response are studied involving material behaviors of viscoplasticity, viscoplasticity–creep and viscoplasticity–relaxation interactions. Experimental data found in previous literature of 304 stainless steels and $Ti_7Al_2Cb_1Ta$ titanium alloy for rate-dependent elasto-plastic response are used for comparison. It is concluded, through comparison with the experimental results, that most rate-dependent elasto-plastic behaviors of materials can be adequately simulated by this endochronic approach.

Furthermore, due to lack of experimental facility, the assumption of eqn (40) can not be supported by any experimental result. However, it has been shown that the theoretical prediction is in good agreement with the experimental data for viscoplasticity–relaxation interaction of $Ti_7Al_2Cb_1Ta$ titanium alloy tested by Kujawski and Krempl (1981). Therefore, the assumption is reasonable.

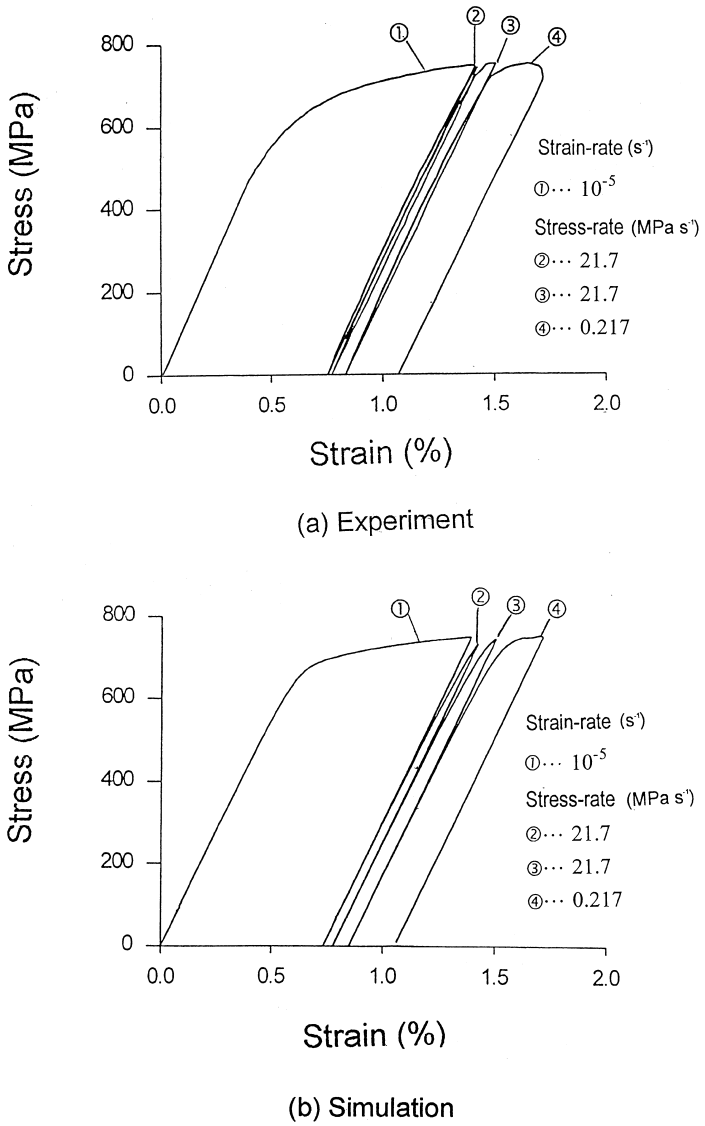

Fig. 7. Experimental and theoretical axial stress–strain curves for $Ti_7Al_2Cb_1Ta$ titanium alloy at different strain rate or stress rates.

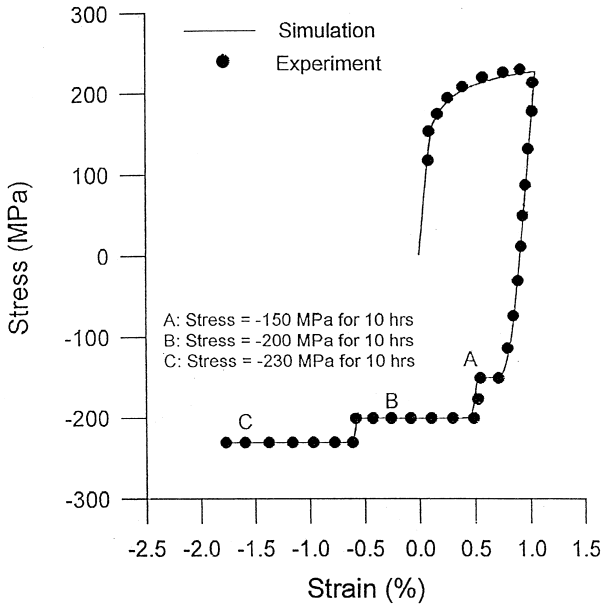

Fig. 8. Experimental and theoretical axial stress–strain curves for 304 stainless steel under three stages of creep.

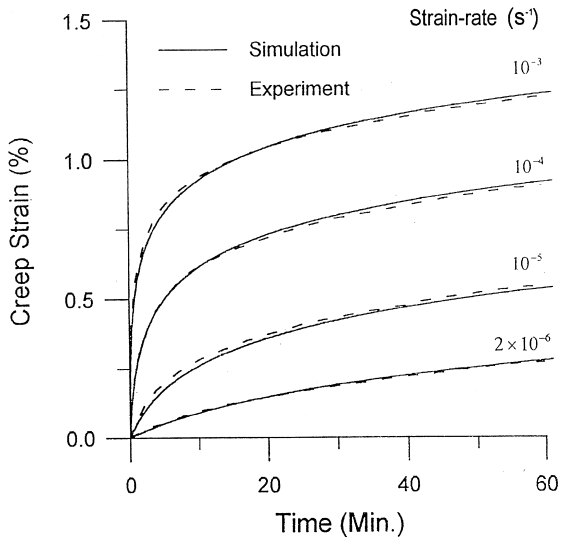

Fig. 9. Experimental and theoretical creep strain vs time curves for 304 stainless steel with different strain rates at preloading.

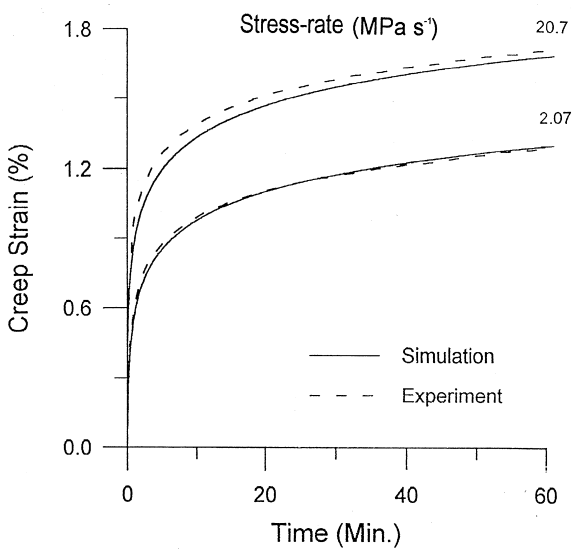

Fig. 10. Experimental and theoretical creep strain vs time curves for 304 stainless steel with different stress rates at preloading.

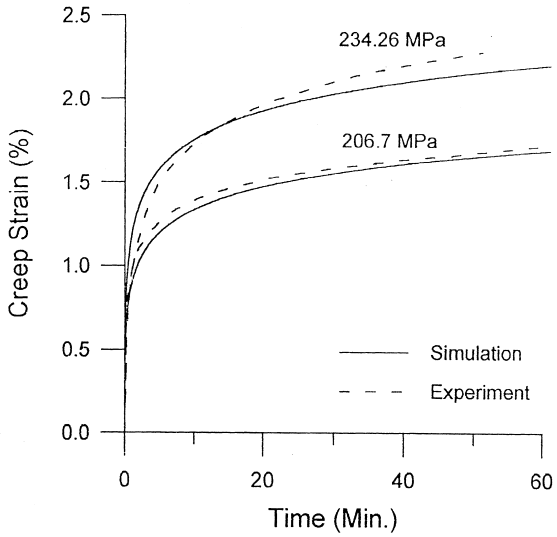

Fig. 11. Experimental and theoretical creep strain vs time curves for 304 stainless steel with constant stress rate at preloading but different holding stress at creep.

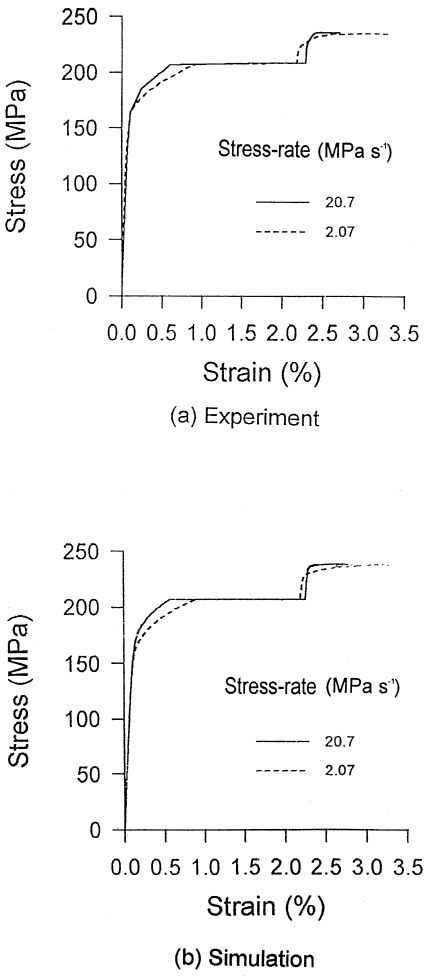

Fig. 12. Experimental and theoretical axial stress–strain curves for 304 stainless steel with two stress rates at two creep stages.

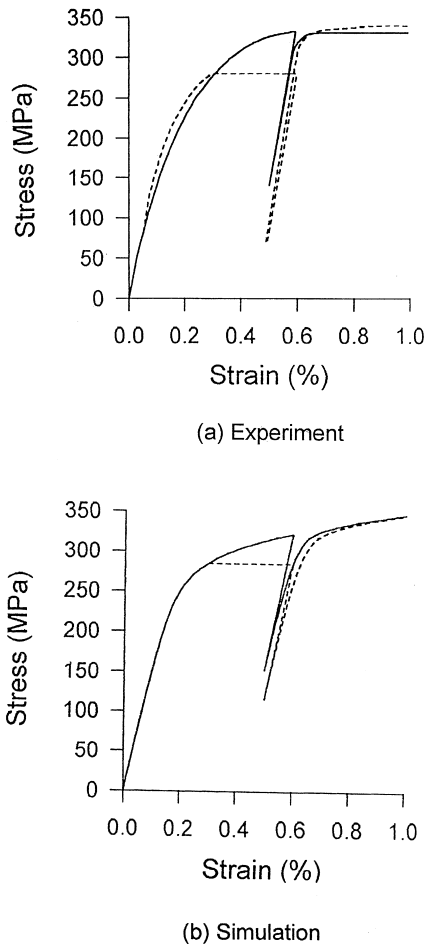

Fig. 13. Experimental and theoretical axial stress–strain curves for 304 stainless steel for the unloading/reloading response following elasto-plastic deformation shown by solid line and the unloading/reloading response following creep shown by dotted line.

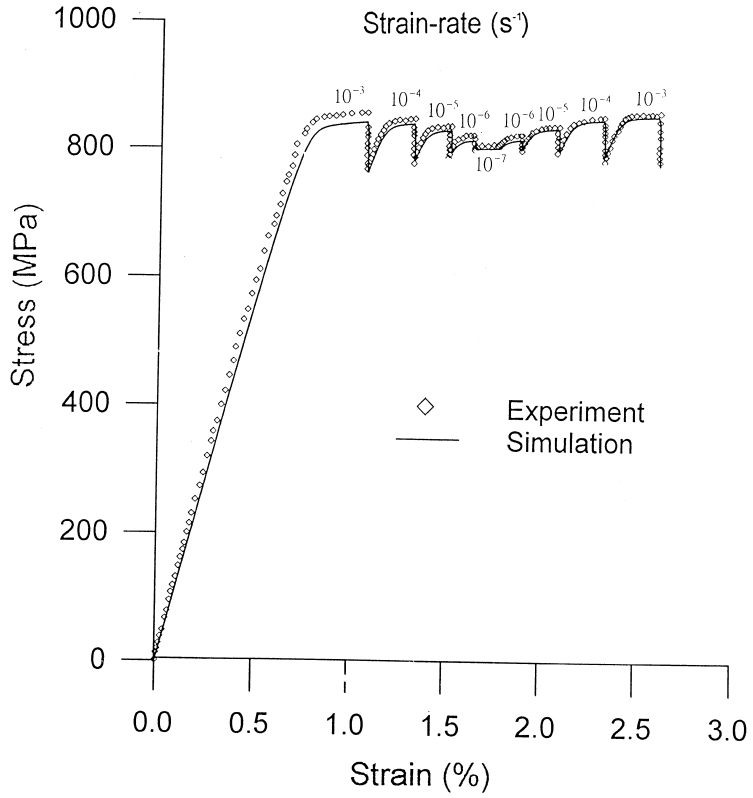

Fig. 14. Experimental and theoretical axial stress–strain response for $Ti_7Al_2Cb_1Ta$ titanium alloy with different strain–rates at preloading following relaxation.

Acknowledgements

The work presented was carried out with the support of National Science Council under grant NSC 86-2212-E-006-007. Its support is gratefully acknowledged.

References

Ellyin, F., Xia, Z., Sasaki, K., 1991. Rate-dependent plastic deformation-experiments and constitutive modelling. Proceeding of PLASTICITY'91, The Third International Symposium on Plasticity and Its Current Applications, Grenoble, France, pp. 439–442.

Fan, J., 1983. A comprehensive numerical study and experimental verification of endochronic plasticity. Ph.D. dissertation. Department of Aerospace Engineering and Applied Mechanics, University of Cincinnati.

Fan, J., Peng, X., 1991. A physically based constitutive description for nonproportional cyclic plasticity, J. Engng. Mater. Tech. 113, 254–262.

Imai, G., Xie, C., 1990. An endochronic constitutive law for static shear behavior of overconsolidated clays, soils and foundations. Japanese Society of Soil Mechanics and Foundation Engineering 30 (1), 65–75.

Ikegami, K., Ni-Itsu, Y., 1983. Experimental evaluation of the interaction effect between plastic and creep deformation. Proceedings of Plasticity Today Symposium, Udine, Italy, pp. 27–30.

Inoue, T., Imatani, S., Sahashi, T., 1985. On the plasticity creep interaction behavior of SUS 304 steel under combined stress state of tension and torsion. Proceedings of the 28th Japan Congress on Material Research, pp. 15–22.

Krempl, E., 1979. An experimental study of room-temperature sensitivity, creep and relaxation of AISI 304 stainless steel. J. Mech. Phys. Solids 27, 363–375.

Kujawski, D., Krempl, E., 1981. The rate(time)-dependent behaviour of $Ti_7Al_2Cb_1Ta$ titanium alloy at room temperature under quasi-static monotonic and cyclic loading. ASME J. Appl. Mech. 48, 55–63.

Kujawski, D., Kallianpur, V., Krempl, E., 1980. Uniaxial creep, cyclic creep and relaxation of AISI type 304 stainless steel at room temperature. J. Mech. Phy. Solids 28, 129–148.

Lee, C.F., 1995. Recent finite element applications of the incremental endochronic plasticity. Int. J. Plasticity 30 (7), 843–864.

Lee, C.F., 1996. A simple endochronic transient creep model of metals with application to variable temperature creep. Int. J. Plasticity 12 (2), 239–253.

Lin, H.C., Wu, H.C., 1976. Strain-rate effect in the endochronic theory of viscoplasticity. J. Appl. Mech. 98, 92–96.

Lin, H.C., Wu, H.C., 1983. On the rate-dependent endochronic theory of viscoplasticity and its application to plastic-wave propagation. Int. J. Solids Struct. 19 (7), 587–599.

Mathison, S.R., Pindera, M.J., Herakovich, C.T., 1991. Nonlinear response of resin matrix laminates using endochronic theory. J. Engng. Mater. Tech. 113, 449–455.

Murakami, J., Read, H.E., 1987. Endochronic plasticity: some basic properties of plastic flow and failure. Int. J. Solids Struct. 23 (1), 133–151.

Murakami, H., Read, H.E., 1989. A second-order numerical scheme for integrating the endochronic plasticity equations. Computers and Structures 31, 663–672.

Nicholas, T., 1971. Strain-rate and strain-rate-history effects in several metals in torsion. Experimental Mechanics 11, 370–374.

Ohashi, Y., Ohno, N., Kawai, M., 1982. Evaluation of creep constitutive equations for type 304 stainless steel under repeated multiaxial loading. J. Engng. Mat. Tech. 104, 159–164.

Pan, W.F., 1997. Finite viscoplastic deformation for metals under torsion. Int. J. Plasticity 13(6–7), 571–586.

Pan, W.F., Chern, C.H., 1997. Endochronic description of viscoplastic behavior of material under multiaxial loading. Int. J. Solids Struct. 34 (17) 2131–2160.

Pan, W.F., Leu, K.T., 1997. Endochronic analysis for viscoplastic collapse of a thin-walled tubes under combined bending and external pressure. JSME Int. Journal 40 (2), 189–199.

Pan, W.F., Lee, T.H., Yeh, W.C., 1996. Endochronic analysis for finite elasto-plastic deformation and application to metal tube under torsion and metal rectangular block under biaxial compression. Int. J. Plasticity 12 (10), 1287–1316.

Peng, X., Ponter, A.R.S., 1993. Extremal properties of endochronic plasticity, part I: extremal path of the constitutive equation without a yield surface, part II: extremal path of the constitutive equation with a yield surface and application. Int. J. Plasticity 9, 551–581.

Valanis, K.C., 1975. On the foundations of the endochronic theory of plasticity. Arch. Mech. 27, 857–872.

Valanis, K.C., 1980. Fundamental consequence of a new intrinsic time measure-plasticity as a limit of the endochronic theory. Arch. Mech. 32, 171–191.

Valanis, K.C., 1984. Continuum foundations of plasticity. ASME J. Engng. Mater. Tech. 106, 367–375.

Valanis, K.C., Lee, C.F., 1984. Endochronic theory of cyclic plasticity with applications. J. Appl. Mech. 51, 367–374.

Valanis, K.C., Read, H.E., 1986. An endochronic plasticity theory for concrete. Mech. Mater. 5, 177–295.

Watanabe, O., Atluri, S.N., 1985. A new endochronic approach to computational elasto-plasticity: an example of cyclically loaded cracked plate. J. Appl. Mech. 52, 857–864.

Watanabe, O., Atluri, S.N., 1986. Constitutive modeling of cyclic plasticity and creep, using an internal time concept. Int. J. Plasticity 2 (2), 107–134.

Wu, H.C., Ho, C.C., 1993. Strain hardening of annealed 304 stainless steel by creep. ASME J. Engng. Mat. Tech. 115, 345–350.

Wu, H.C., Ho, C.C., 1995. An investigation of transient creep by means of endochronic viscoplasticity and experiment. ASME J. Engng. Mat. Tech. 117, 260–267.

Wu, H.C., Yao, J.C., 1981. Investigation of creep by using of closed loop servo-hydraulic test system. Report G302-81-001, Division of Material Engineering, The University of Iowa.

Wu, H.C., Yip, M.C., 1980. Strain rate and strain-rate history effects on the dynamic behavior of metallic materials. Int. J. Solids Struct. 16, 515–536.

Wu, H.C., Yip, M.C., 1981. Endochronic description of cyclic hardening behavior for metallic material. J. Engng. Mater. Tech. 103, 212–217.

Wu, H.C., Lu, J.K., Pan, W.F., 1995. Endochronic equations for finite plastic deformation and application to metal tube under torsion. Int. J. Solids Struct. **32**(8/9), 1079–1097.

Wu, H.C., Wang, T.P., Pan, W.F., Xu, Z.Y., 1990. Cyclic stress–strain response of porous aluminum. Int. J. Plasticity 6, 207–230.

Xia, Z., Ellyin, F., 1993. An experimental study on the effect of prior plastic straining creep behavior of 304 stainless steel. ASME J. Engng. Mat. Tech. 115, 200–203.

Yamada, H., Li, C.Y., 1973. Stress relaxation and mechanical equation of state in austenitic stainless steel. Met. Trans. 4, 2133–2139.

Yoshida, F., 1989. Viscoplastic behavior of SUS 304 stainless steel under cyclic loading at room temperature and its phenomenological description. In: Khan, A.S., Tokuda, M. (Eds.), Proceeding of PLASTICITY'89, the Second International Symposium on Plasticity and its Current Applications. Mei, Japan, pp. 277–280.